Letters in Applied NanoBioScience
Open-Access Journal (ISSN: 2284-6808)

Article
Volume 13, Issue 2, 2024, 53
https://doi.org/10.33263/LIANBS132.053

Synthesis of Fluorescent Probe for the Detection of Pb^{2+} ions and Interpretation of its Binding Affinities with BSA, DNA, and p53 Cancer Mutant Protein using Molecular Docking Studies

Prema Mahadeva [1], Revanasiddappa Hosakere Doddarevanna [1,*]

[1] Department of Studies in Chemistry, University of Mysore, Manasagangotri, Mysuru-570006, India
* Correspondence: hdrevanasiddappa@yahoo.com (R.H.D.);

Scopus Author ID 7004879365
Received: 24.02.2023; Accepted: 4.04.2023; Published: 30.06.2024

Abstract: In this study, a thiosemicarbazone Schiff base, (E)-2-(3-phenoxybenzylidene) hydrazine-1-carbothioamide) [Probe-L] has been synthesized and has primarily been characterized by physical methods and structurally by spectroscopic methods such as LC-MS, FT-IR and NMR spectroscopy. The Probe-L exhibited turn-on fluorescent behavior with Pb^{2+} ions, and it showed fluorescent enhancement upon binding with Pb^{2+} ions in acetonitrile solution. The binding constant (K_b) and the Stern-Volmer quenching constant (K_{sv}) are calculated. The interaction of the synthesized ligand with bovine serum albumin (BSA) and DNA (CT-DNA) has been studied using emission and absorption techniques. The interactions of ligands with BSA, DNA, and p53 cancer mutant protein have been further supported by molecular docking studies. The binding scores represent the strength of binding affinity.

Keywords: Fluorescence, CT-DNA, BSA, molecular docking, probe, enhancement

1. Introduction

Heavy metal ions are a ubiquitous environmental pollutant that causes serious health hazards to humanity [1]. These metals are, in fact, toxic and carcinogenic. They accumulate in tissue and cause serious diseases and disorders. Heavy metal contamination is a growing crisis that many developing countries are facing today. Lead toxicity has been known to mankind for centuries [2-4]. Lead ion is considered a major environmental pollutant due to its non-biodegradability, long half-life, bio-accumulation, and high health risk to humanity. Although Pb^{2+} ions concentration is very low in foods, its accumulation propagates through the food chain and threatens people's health. The prolonged exposure to Pb^{2+} resulted in various disorders [5]. The human health risks such as anemia, muscle paralysis, memory loss, cardiovascular disease, and mental preparedness are due to inhalation, absorption through the skin, contact with Pb^{2+} polluted soil, and exposure to dust containing Pb^{2+} ions sources.

Therefore, quantitative and sensitive detection of Pb^{2+} ions is important, particularly in an aqueous environment. Many technologies have been developed to detect lead ions [Pb^{2+}]. ELISA has been developed as an effective tool for detecting lead ions. The detection of heavy metal ions using LFA (Lateral flow assay) has emerged as a powerful analysis platform. Apart from these, atomic absorption spectroscopy (AAS), inductively coupled plasma atomic

emission spectroscopy(ICP-AES), Graphene furnace atomic absorption spectroscopy(GFAAS), surface-enhanced Raman spectroscopy, colorimetry, biochemical and electrochemical techniques such as anodic stripping voltammetry, cathodic stripping voltammetry, adsorptive stripping voltammetry but these methods are time-consuming, required expensive, sophisticated equipment and many have complicated sample pre-treatment. Therefore, developing a novel method for Pb^{2+} real-time sampling is highly desirable. Recently, fluorescent spectroscopy has attracted considerable interest due to its simplicity, low cost, high sensitivity, and selectivity [6-12]. Fluorescent molecular probes are essential research tools that can provide sensitive and selective detection of chemical species in real-time sensing targets. Fluorescent probes serve as a tool to understand the biological activities in animals and plants that occur due to environmental uptake [13,14]. Herein, report the synthesis of a new fluorescent probe–L derived from thiosemicarbazide conjugated with a 3-phenoxybenzaldehyde. Probe-L could selectively detect lead based on the turn-on fluorescence mechanism among other metal ions. The synthesis of Probe-L is shown in Scheme-1. The structure of probe-L was confirmed by Mass spectra, 1H-NMR, 13C-NMR, and FT- IR spectra.

2. Experimental

2.1. Materials and methods.

All reagents, including BSA and CT-DNA were brought from Sigma-Aldrich and were used without further purification. Solutions of 30 µM Probe-L and 10 µM tris HCl buffer (pH 7) were used to prepare protein solutions and for fluorescent titration experiments.

2.1.1. Preparation of stock solution.

Standard solution of Probe-L was prepared in CH_3CN: H_2O (v/v=3:7. Standard aqueous solution of metal ions such as Fe(II), Al(III), Cu(II), Co(III), Zn(II), Hg(II), Pb(II), Cd(II) and Ni(II) (10^{-4} M) [nitrate and chloride salts of transition metals] were prepared and diluted accordingly before experimentation.

2.1.2. Sensing experiments.

The sensing behavior of different metal ions was examined by taking 3 mL aliquots of standard solutions of Probe-L (30µM) in a cuvette, and then metal ion solutions (10µM) were added accordingly.

2.1.3. Instrumentation.

The melting point determination was uncorrected in an open capillary tube using a precision digi-melting point apparatus. Mass spectra of synthesized compounds were recorded using 1 2010 EV LCMS Shimadzu spectrometer. The ^{1}H and ^{13}C NMR spectra were recorded using Bruker Advance 500 (USA) spectrometer, and chemical shifts are given in ppm with residual DMSO as reference. FT-IR spectra were recorded by PerkinElmer Spectrum Version 10.03.09 spectrophotometer in the range of 4000-400 cm^{-1}. UV-visible spectra were recorded by using DU 730 Spectrophotometer, S/N 1333105, Instrument version: 1.05, with a diode array detector. Fluorescence spectra were measured on a Varioskan Flash (4.00.53)

Fluorescence spectrophotometer. The pH measurements were carried out using Eutech pH-700 instrument.

2.2. Synthesis of Probe – L.

Probe-L was synthesized by the 1:1 condensation of thiosemicarbazide with 3-phenoxy benzaldehyde. Add a solution of thiosemicarbazide (0.15 g, 0.016 mole) in 8 mL of hot ethanol, 3-phenoxy benzaldehyde (0.326g, 0.0016 mole) in 10 mL ethanol was refluxed for 6 h. After cooling to room temperature, the yellow solid precipitate of Probe - L was obtained. The precipitate was filtered and washed with hot ethanol before being dried in a desiccator. The progress of the reaction was monitored using TLC [n-hexane: ethyl acetate = 8:2]. A pure synthesized compound was obtained from continuous recrystallization. Yield =87%, mp = 174 °C. The synthesis of Probe-L is given in Scheme-1.

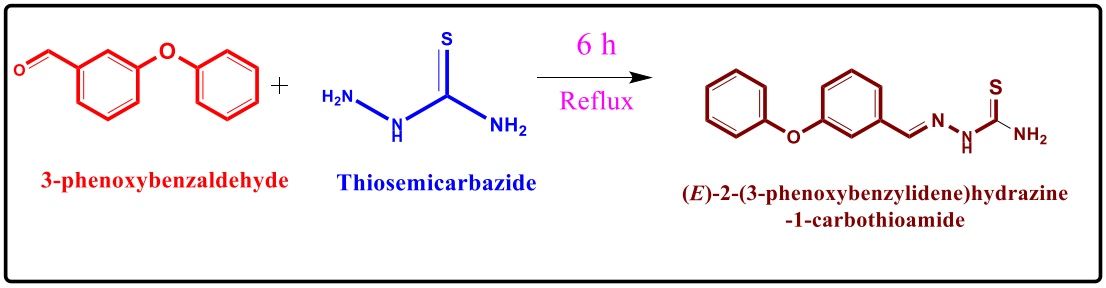

Scheme 1. Synthesis of Probe-L.

3. Results and Discussion

3.1. NMR spectroscopy and mass spectrometry

The ^{1}H NMR and ^{13}C NMR spectra of Probe-L were shown in S1 and S2, respectively. A sharp singlet that integrates as one hydrogen at δ = 8.07 ppm is assigned to azomethine (-CH=N-). The absence of coupling interactions due to the lack of availability of protons on neighboring atoms renders singlet peaks for the imine protons. Another singlet at δ = 11.67 ppm can be attributed to the proton attached to N. The multiple signals of Ar-H were observed in the range of 7.06 – 7.48 ppm. The structure of the Probe-L was further evaluated by ^{13}C NMR. The signals at δ = 146.8 ppm and δ = 178.5 ppm are attributed to carbon of azomethine and carbon of C=S, respectively. The peaks observed between δ = 118.9 – 157.1 ppm show aromatic ring carbons. The formation of Probe-L was confirmed through mass spectrometry. The mass spectrum of Probe-L and its complex with Pb^{2+} were depicted in S3 and S4, respectively. The molecular ion peak at m/z =270[M-1] is consistent with the mass of the Probe-L (S3), and peaks at m/z = 477 and 749 correspond to 1:1 and 1:2 binding of Probe-L with Pb^{2+} (S4)[15].

3.2. FT-IR spectra.

The FT-IR spectra of Probe-L and its complex with Pb^{2+} were shown in S5 and S6, respectively. The characteristic band 1697cm^{-1} is assigned to (-C=N-) stretching frequency. The IR spectrum of Probe-L showed a band at 3400 cm^{-1} due to (-NH) stretching vibrations (S5). Upon complexation, the bands of the imine group and (-NH) group displayed a shift to lower wavenumber (1531cm^{-1}) and (3384 cm^{-1}) as compared to Probe-L spectra alone indicates that these groups involved in complexation (S6)[16].

3.3. UV-visible absorption studies of Probe-L with different metal ions.

The sensing ability of Probe-L with different metal ions was studied by UV-visible spectroscopy in CH3CN. As shown in Fig-1, UV-vis absorption spectra of Probe-L showed an absorption band at a longer wavelength at 345 nm corresponding to n-π* transition. The electronic absorption spectra of the compound display high energy bands in the region ~ 266-270 nm, corresponding to π- π* transition. The addition of Ni^{2+} and Zn^{2+} to the solution showed an absorption band at 370 and 375 nm, respectively. In the presence of Cd^{2+}, Hg^{2+}, and Al^{3+}, the absorption bands are also shifted. This indicates that there is a partial interaction of these ions with Probe–L. The Probe-L exhibits a weak fluorescence emission band at 500 nm, which is shown in Fig-2. The photographs of Probe-L interaction with Pb^{2+} and with different metal ions under UV lamp were shown in Fig 3(a) and 3(b), respectively [17].

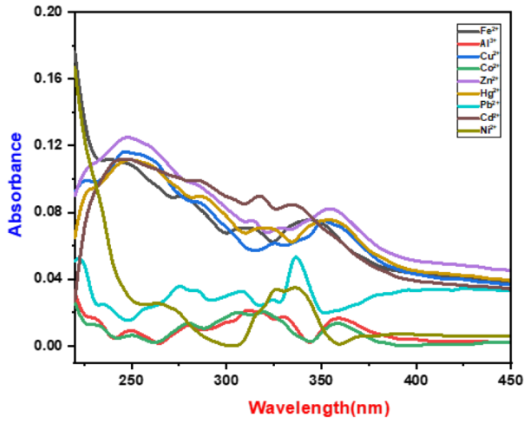

Figure 1. UV-visible spectra of Probe-L recorded in CH_3CN after the addition of different metal ions.

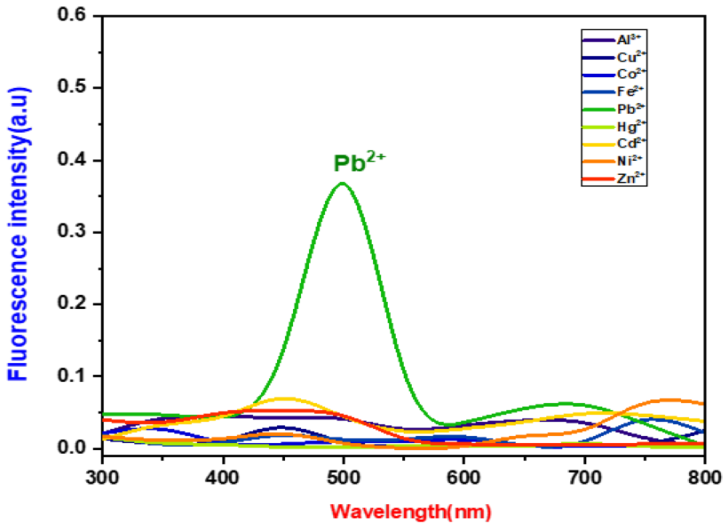

Figure 2. Fluorescence emission spectra of Probe-L in the presence of different metal ions (10µM).

3(a) 3(b)

Figure 3. Photographs under UV lamp of Probe-L interacting with Pb^{2+} **(a)** and different metal ions **(b).**

3.4. Fluorescence titrations and binding studies.

3.4.1. Fluorescence titrations.

To further investigate the sensing properties of Probe-L, fluorescence titration of Probe-L was carried out with different concentrations of Pb^{2+}. Fig-4, showed changes in the fluorescence intensity of Probe-L with the addition of increasing concentrations of Pb2+ to a solution of Probe-L in CH_3CN. The fluorescence intensity of Probe-L at 500 nm was enhanced gradually until the concentration of 10µM. The result indicated that the Probe-L could form a stable complex with Pb^{2+}. The association constant was determined by Stern-Volmer (S-V) plot using a modified Stern-Volmer equation (eq-1)

$$\frac{F0}{\Delta F} = \frac{1}{fa} + \frac{1}{faKa}[Q] \quad (1)$$

Where,

F0 is the initial fluorescence intensity in the absence of a quencher, and fluorescence intensity in the presence of a quencher is termed as F. Ka is Stern-Volmer constant, [Q] is the quencher concentration. fa is the initial fluorescence in fractions, which is accessible to the quencher. The Stern-Volmer plot of Probe-L with Pb2+ ions is represented in Fig-5. The binding constant calculated by this method was found to be 1.022 × 103M-1 [18-19].

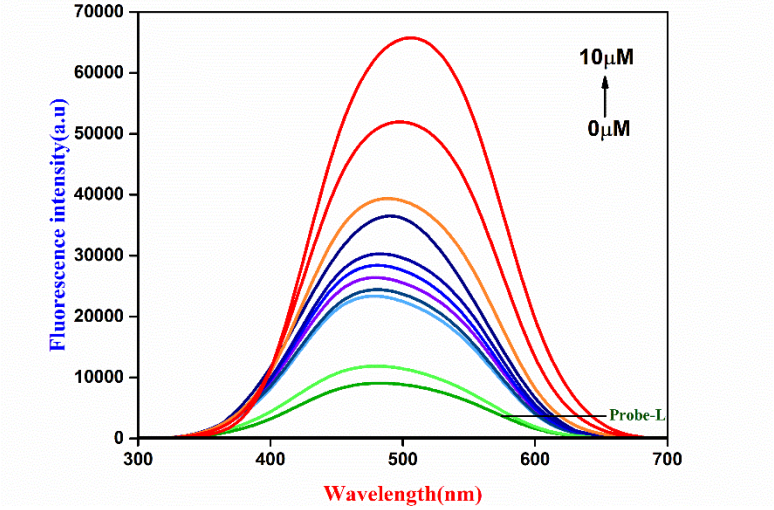

Figure 4. Fluorescence spectra of Probe-L (30µM) in CH_3CN upon addition of increasing concentrations of Pb^{2+}.

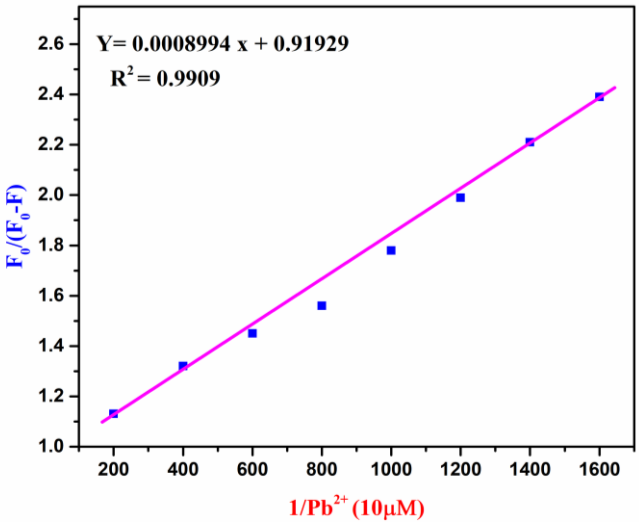

Figure 5. Binding studies of Probe-L using Stern Volmer plot.

3.5. Metal ion competitive study.

The competitive binding studies were conducted to understand the recognition ability of Probe-L in the presence of other coexisting metal ions, and the corresponding fluorescence intensities were recorded (Fig-6). The fluorophore Probe-L(30µM) with 10 equivalents of Pb2+ was treated with the same equivalent of other metal ions. The resulting emission intensities indicated that the addition of these competitive cations did not affect the emission of the Probe-L-Pb^{2+} complex (red bars in Fig-6). The data concludes that Probe-L is very much selective and sensitive towards Pb^{2+} ions, which suggests that the background metal ions showed a very low interference in the detection of Pb^{2+} metal ions and LOD and LOQ, obtained to be 3.4 x 10-6 M and 1.04 x10-7, respectively [20-21].

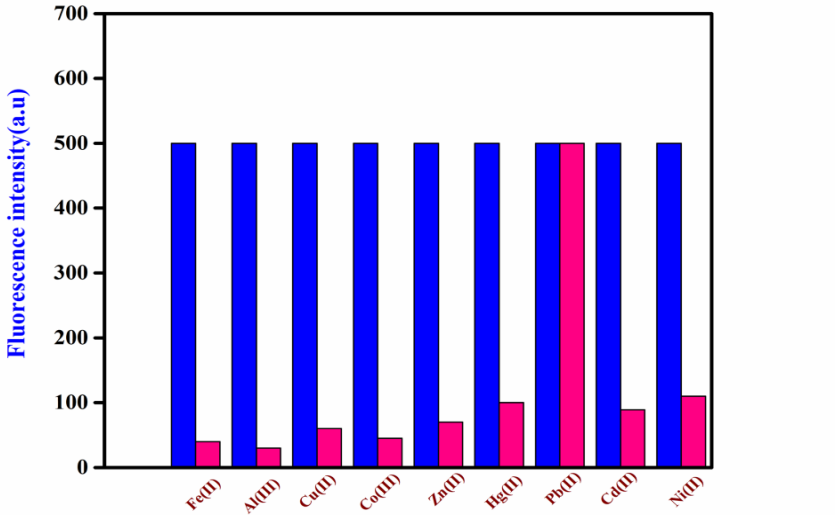

Figure 6. Selectivity profile of Probe-L for Pb^{2+} in CH_3CN: H_2O solution (v/v= 3:7; HEPES buffer, pH=7.2). The red bars indicate the emission intensity of the solution of Probe-L(30µM) with 10 µM of different metal ions, while the blue bars indicate the emission intensity after the addition of different metal ions to the solution containing Probe-L and 10 µM of Pb^{2+}

3.6. Binding stoichiometry.

In order to confirm the binding stoichiometry between Probe-L and Pb2+, Job's plot and absorption titration spectra were carried out. As shown in Fig-7, a Job's plot indicated a 1:2 stoichiometric complexation of Probe-L with Pb2+. The Probe–L exhibited maximum fluorescence intensity at a mole fraction of 0.6, which is evidence of 1:2 stoichiometric complexation between Probe- L and Pb^{2+} [22].

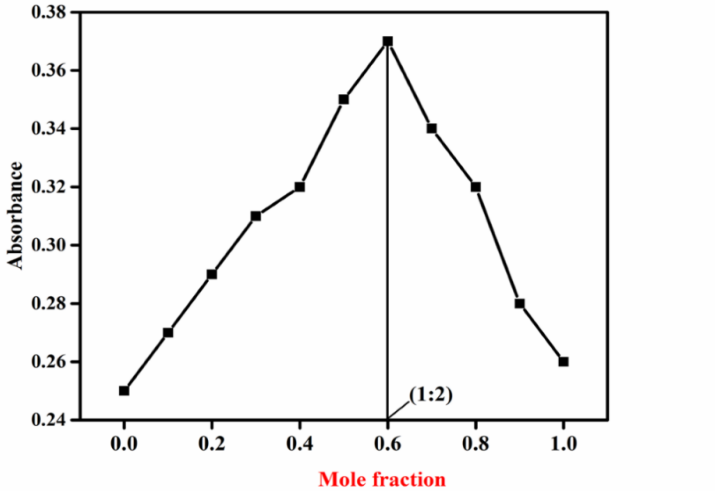

Figura 7. The Job's plot examined between Probe-L and Pb^{2+}.

3.7. Effect of pH.

The effect of pH on the fluorescence of Probe –L with Pb^{2+} was investigated in acetonitrile - water solution (1:9). The pH of the solution was adjusted by using NaOH and HCl as shown in Fig- 8, the Probe – L - Pb^{2+} shows very good fluorescence behavior in the pH range of 5.0 to 13.0 as observed against weak fluorescence behavior in the pH range of 1.0 - 4.0 due to the increased interference of H+ ions. The result of the pH titration indicates that the Probe –L could be used to determine Pb^{2+} ions under common environmental conditions [23].

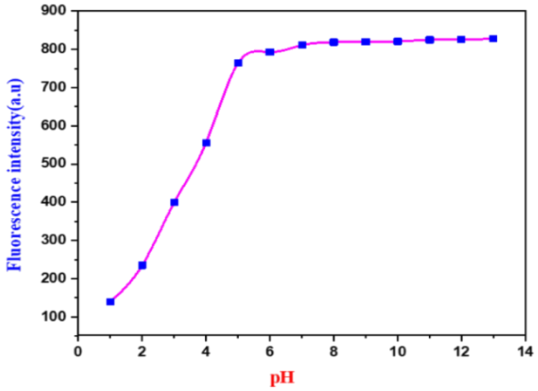

Figure 8. The variation in fluorescence intensity with the pH of the Probe –L(30µM) in the presence of Pb^{2+}.

3.8. Bioassay studies.

3.8.1. BSA binding studies of Probe-L.

Electronic absorption titration

The BSA molecule consists of 583 amino acids bound in a single chain cross-linked with 17 cysteine residues and has a molecular mass of 66000 Da. BSA is the most studied serum albumin due to its structural similarity to human serum albumin (HAS). Human serum albumin contains one tryptophane at the Trp-214 position, while BSA contains two tryptophan residues, Trp 134 and Trp 214 [24]. To examine the BSA interactions of Probe-L, 10µM BSA solution was prepared in tris-HCl buffer (pH: 7.0). The absorption titration was carried out by keeping the BSA concentration constant and varying the concentrations of Probe-L. After 10 min of incubation at room temperature, absorbance was measured for each solution in the range of 200 to 600 nm wavelength, and λmax was recorded at 310 nm, as shown in Fig-9. The plot shown in Fig-10 is 1/(A-A0) v/s 1/[L] is a linear plot [where A0 is the initial absorbance of the BSA at 310 nm, A is the absorbance of BSA at different concentrations of Probe- L] is used to determine the binding constant (Kb) [25-26].

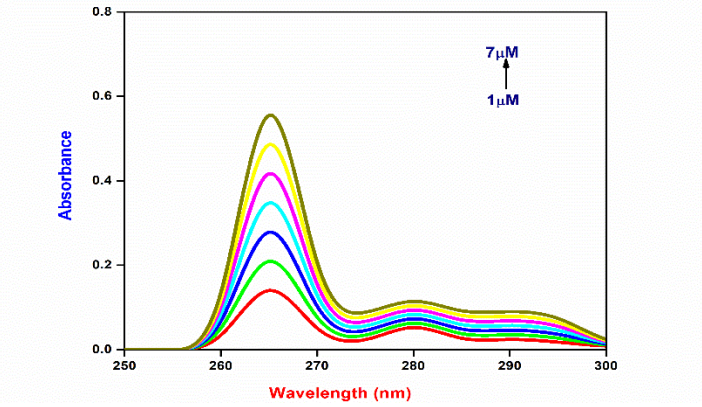

Figure 9. Electronic absorption spectra of BSA in the presence of Probe-L with increasing concentrations in the range from 1-7 µM.

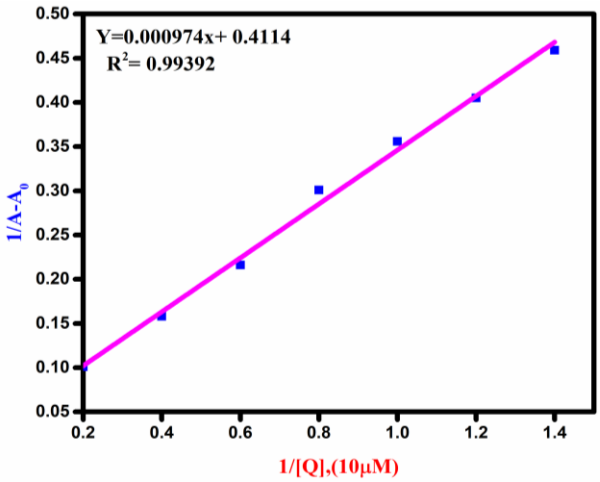

Figure 10, Stern-Volmer plot of BSA with different concentrations of Probe- L.

3.8.2. DNA binding studies.

Electronic absorption titrations

Absorption titration experiments were made using different concentrations of CT-DNA while keeping the Probe-L concentration constant. After 10 min of incubation at 4 ^{o}C each sample solution was scanned from 200 to 800 nm and which is shown in Fig-11. The UV spectral data were fitted into the Wolf-Shimer equation to obtain the intrinsic binding constant (Kb).

$$\frac{[DNA]}{\epsilon a-\epsilon b}=\frac{[DNA]}{\epsilon b-\epsilon f}+\frac{1}{Kb(\epsilon b-\epsilon f)} \quad (1)$$

Where, [DNA] is the concentration of DNA in base pairs, ϵa is the apparent extinction coefficient (Aobs/ [Probe-L]), ϵb is the extinction coefficient of the Probe-L in the fully bound form, and the extinction coefficient for the Probe-L is ϵf. The plot of [DNA]/ϵa-ϵf v/s [DNA] is a linear curve shown in Fig- 12, and the binding constant (Kb) can be obtained by the ratio of intercept to the slope [27-28].

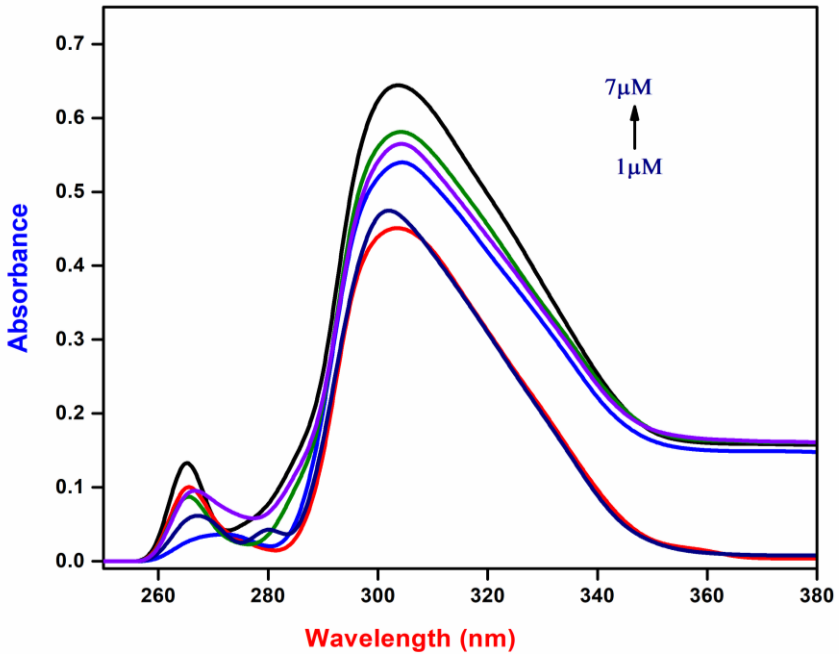

Figure 11. Electronic absorption spectra of DNA upon addition of different concentrations of Probe-L.

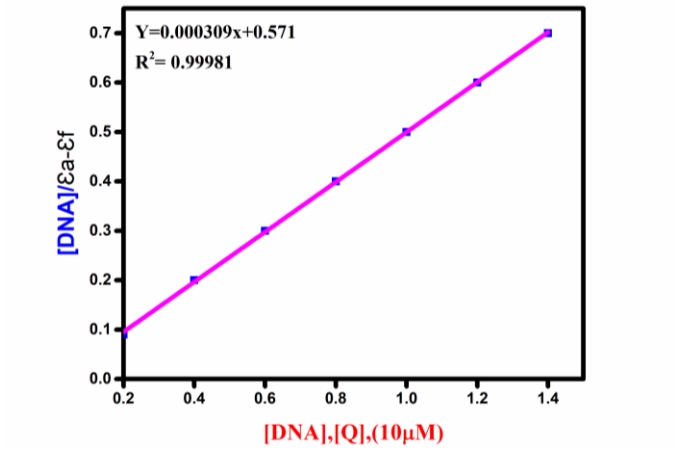

Figure 12. Stern-Volmer plot of Probe-L with increasing concentrations of DNA.

Fluorometric studies

The fluorescence spectra of the reaction mixture were recorded between 400 to 500 nm at the excitation wavelength of 310 nm for BSA binding studies and between 450 to 650 nm at the excitation wavelength of 280 nm for DNA binding studies shown in Fig- 13 and Fig-14, respectively. The fluorescence quenching efficiency is evaluated according to the classical Stern-Volmer equation 2. The binding constant (Kb) and number of binding sites (n) can be determined from emission spectra with equation 3. The Stern-Volmer plot of log[(F0-F)/F] v/s log [Q] is a straight line which is evident in Fig-15 and Fig-16, respectively.

$$\frac{F0}{F} = 1 + ksv\,Q \quad (2)$$

$$\log\left(\frac{F0-F}{F}\right) = \log kb + n\log[Q] \quad (3)$$

The fluorescence intensities in the absence of a quencher are given as F0, and in the presence of a quencher is termed F. The concentration of the quencher and Stern-Volmer quenching constant are represented as Q and Ksv, respectively. The binding constant (Kb) for BSA and DNA binding with the Probe-L was found to be 1.221^{x} 103, and 1.374 ^{x} 103, respectively. The Stern-Volmer quenching constant (Ksv) values were obtained to be 2.414 ^{x} 103 and 2.039 ^{x} 103 for BSA and DNA binding with the Probe-L, respectively. The Gibbs free energy (ΔG) of formation can also be calculated by using the equation,

ΔG = −RT ln (KD)

Where, KD = 1/ Ka is the dissociation constant, R is the universal gas constant, and T is the temperature in Kelvin. The binding properties of Probe-L with Pb2+, BSA, and DNA are tabulated in Table 1 [29-31].

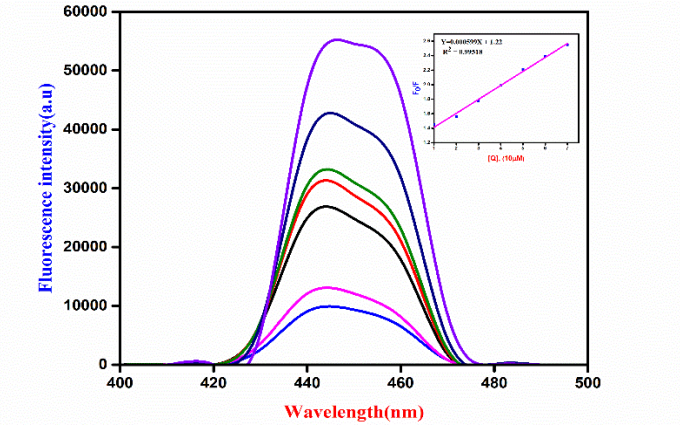

Figure 13. Fluorescence emission spectra of BSA in the presence of Probe-L with increasing concentrations in the range from 1-7 μM; λexc= 310 nm; λems=445nm.

Inset: A plot of F_0/F v/s [Q]

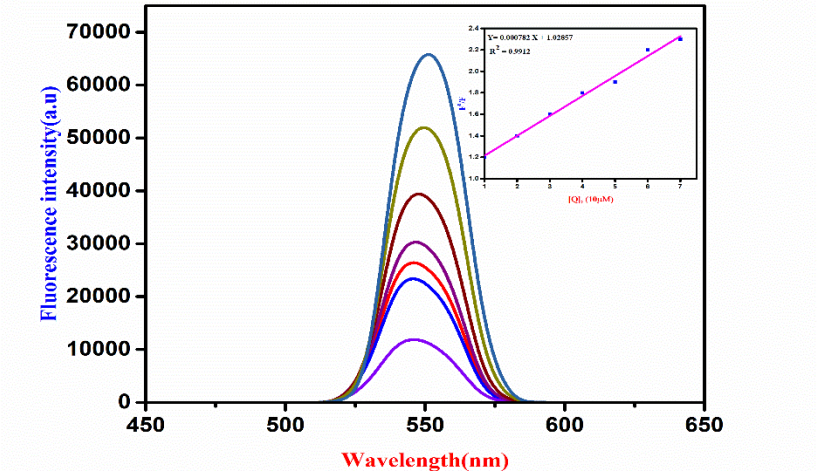

Figure 14. Fluorescence emission spectra of DNA in the presence of Probe-L with increasing concentrations in the range from 1-7 µM; λexc= 280nm; λems=540nm.

Inset: A plot of F_0/F v/s [Q]

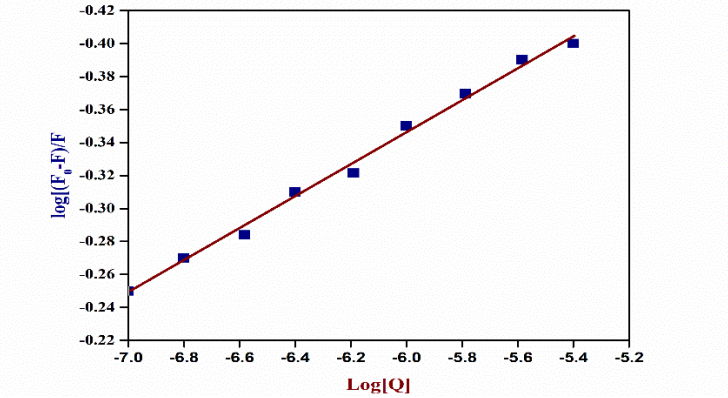

Figure 15. Stern- Volmer plot of log[(F_0-F)/F] v/s log [Q](BSA).

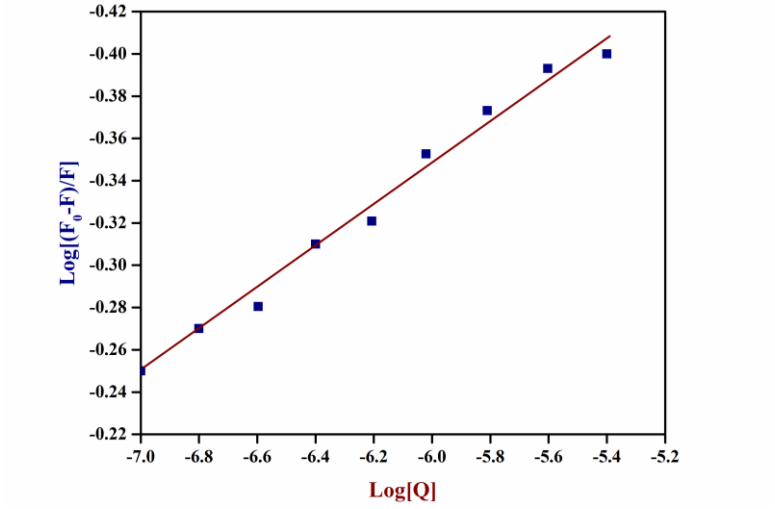

Figure 16. Stern-Volmer plot of log[(F_0-F)/F] v/s log [Q](DNA).

Table 1. The association constant (Ka), dissociation constant (K_D), Gibb's free energy (ΔG) of Probe-L with Pb^{2+}, BSA, DNA, and corresponding linear correlation co-efficient R^2 data.

Complex	Ka (M^{-1})	K_D (mM)	ΔG(KJ/mol)	R^2
Probe-L: Pb^{2+}	1022.11	0.978	-7.594	0.9909
Probe-L: BSA	2036.72	0.491	-8.255	0.9951
Probe-L: DNA	1315.3	0.76	-7.779	0.9912

3.9. Molecular docking studies.

Molecular docking studies were performed to interpret the non-covalent interaction of the synthesized ligand [Probe-L] with bovine serum albumin (BSA), deoxyribonucleic acid (DNA), and P53 cancer mutant protein. The proteins and DNA structures were retrieved from Protein Data Bank [PDB ID: BSA (6QS9); DNA (1BNA) and P53 cancer mutant protein(4L09)] [32]. Molecular docking simulations were executed by PyRx along with Autodock tools such as Vina Wizard [33]. The PyMOL and Discovery studio visualizer was used to analyze the results. Hydrogen bond interaction plots were obtained by 2D-PLOT [34-35].

The receptors bovine serum albumin, transport protein 6QS9, 1BNA, and 4L09 were prepared by deleting the water molecules and hetero atoms. Polar hydrogen and Kollman charges were added. The grid box was generated with cell dimensions of 96.712 × 81.0870 × 82.3103 A0 for 6QS9; 26.9953 × 29.1469 × 38.3763A0 for 1BNA and 49.3170 × 39.9849 × 47.2022 A0 for 4L09, respectively. Ligand coordinates were prepared by adding polar hydrogens. After performing docking simulations, the binding energy values for Probe-L with 6QS9, 1BNA, and 4L09 were found to be -7.4, -5.0, and -6.0 kcal/mol, respectively. The results suggest the stronger, more efficient binding of Probe-L with BSA than DNA and P53 cancer mutant protein [36].

The best-docked conformer of Probe-L with BSA is shown in Fig-17. The ligand is deeply embedded into the cavity of BSA. All the interactions are shown in the 2D interaction plot and hydrogen bonding plot (Fig-18a and Fig-18b). The amine group in the ligand contributes to the formation of hydrogen bond contact with the residue ASP-108 and ARG-144, respectively. The pi-alkyl interactions were observed between the phenol ring of the ligand and amino acids ALA-193, ARG-196, and ILE-455. The pi-sigma interaction was observed between the phenol ring of the ligand and the amino acid ARG-458[37].

The most stable docked conformer of Probe-L with 1BNA is shown in Fig-19. The Probe-L is strongly binding to DNA at the major groove region. The non-covalent interactions involved in the Probe-L-DNA are conventional hydrogen bonds along with carbon-hydrogen short contacts. All the interactions are represented in the 2D-interaction plot shown in Fig-20(a) and the hydrophobic plot shown in Fig-20(b). The nucleotides DT-A:7 and DT-A: are involved in hydrogen bonding with nitrogen atoms, and DA-A:6 is involved in hydrogen bonding with oxygen atoms of the phenyl ring, respectively. The nucleotide DA-A:5 is involved in pi-pi interaction with the phenyl ring. *In silico* studies confirm that the Probe-L exhibited a good binding affinity for the targets BSA and DNA, which are also verified with experimental binding studies. (see section view).

The best possible interaction of Probe-L with P53 cancer mutant protein (4L09) is shown in Fig-21. The Probe-L strongly interacts with the residues Phe: A-113, Tyr: A:32, Asn: A-113 and Ser: A-269 by conventional hydrogen bonding, Trp: A-146 by pi-pi T-shaped interaction, Tyr: A-126 by pi-pi stacked interaction, Pro: A-128 by pi-alkyl interaction and Gly: A-112 by carbon-hydrogen bond interactions which is evident in 2D interaction plot (Fig-22). The hydrogen bond interaction of Probe-L with the P53 cancer mutant protein is shown in Fig-23.

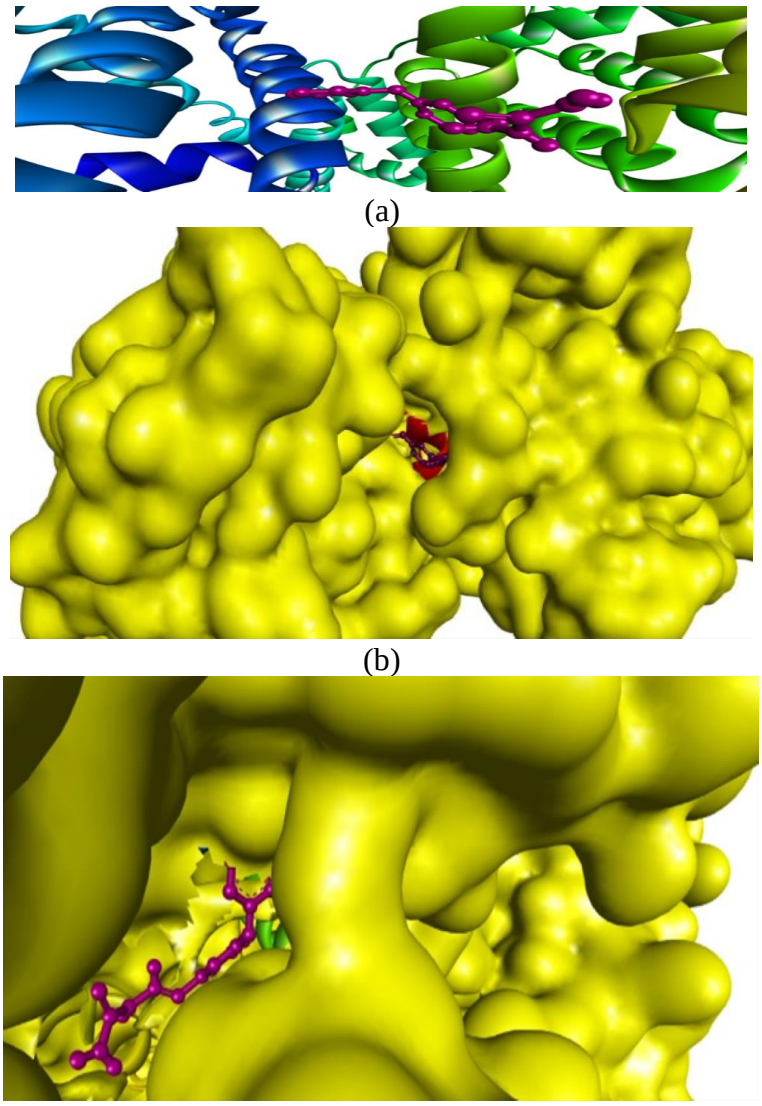

(a)

(b)

(c)

Figure 17. Best docked pose for BSA –Probe-L showed in 3D ribbon representation of protein BSA with docked ligand **(a)** and 3D molecular surface representation with docked ligand (magenta colored stick representation) disposed at the active site: **(b)** Full view **(c)** Close up view.

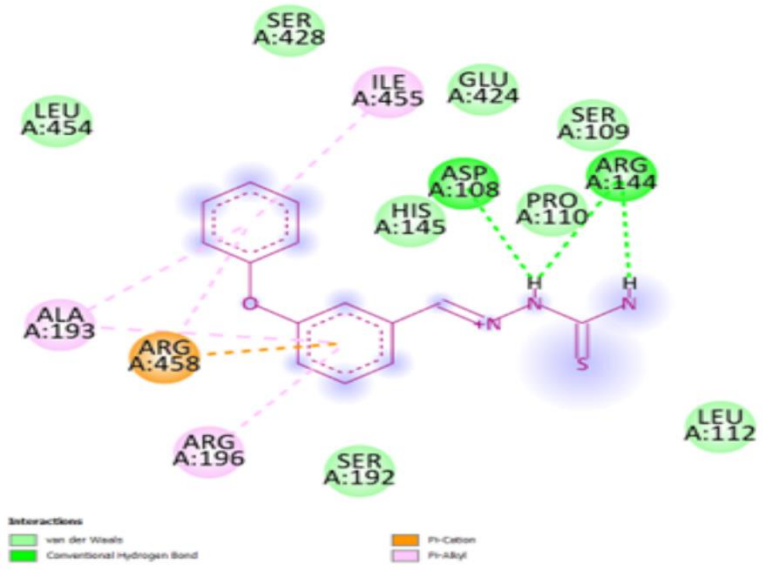

(a)

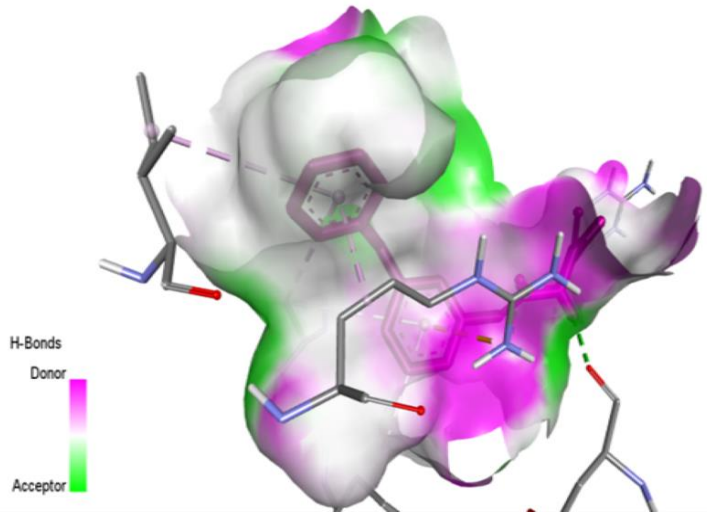

(b)

Figure 18. 2D-plot showing all the interactions between the protein BSA and the Probe-L **(a);** Hydrogen bond interaction plot **(b).**

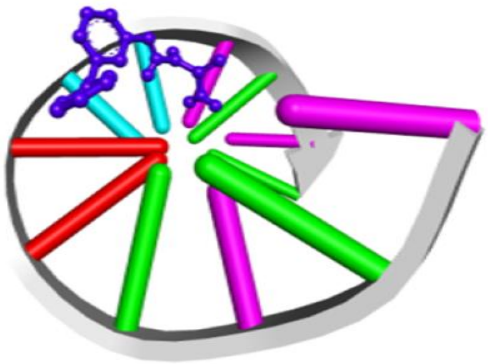

Figure 19. Cartoon representation of the best-docked pose of Probe-L with receptor DNA.

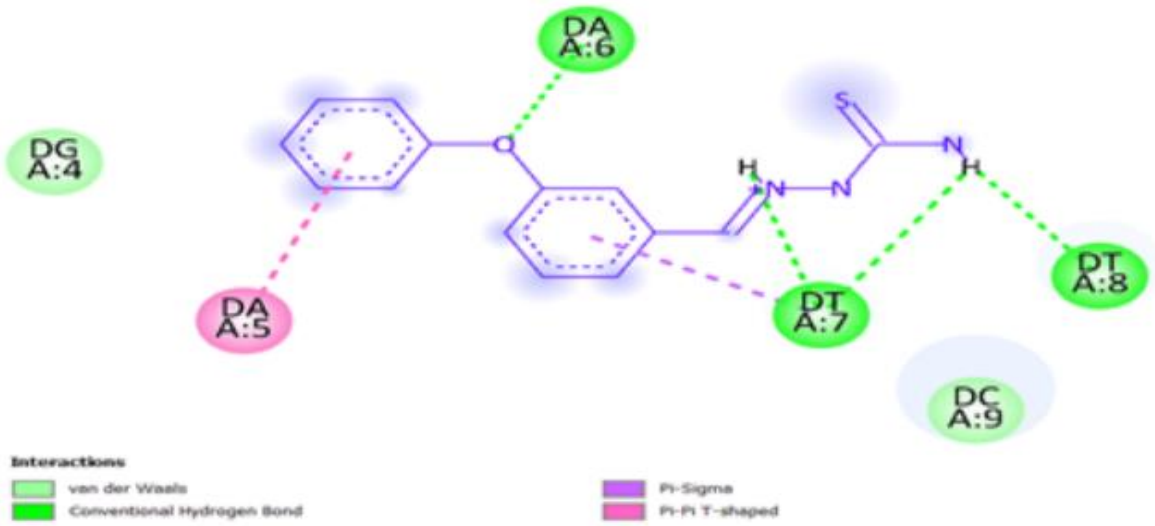

Figure 20. (a) 2D-plot showing all the interactions between the protein DNA and Probe-L.

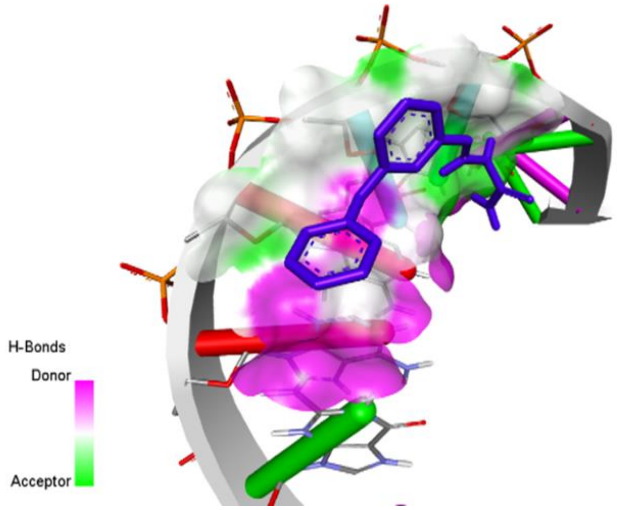

Figure 20. (b) Hydrogen bond interaction plot.

Figure 21. The stable docked pose for Probe-L– 4L09 (P53 cancer mutant protein) is shown in 3D ribbon representation of the P53 cancer mutant protein.

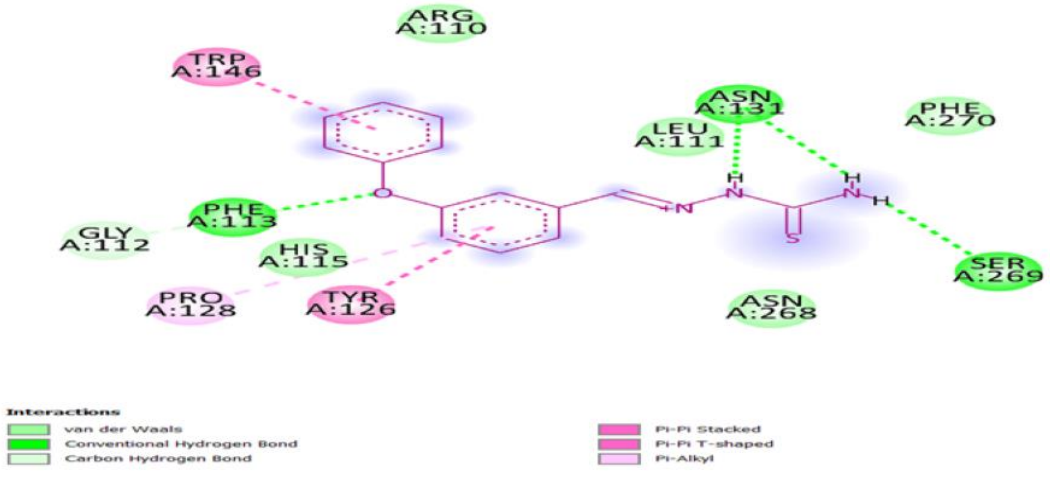

Figure 22. 2D-plot showing the interactions between the Probe-L and p53 cancer cell mutant.

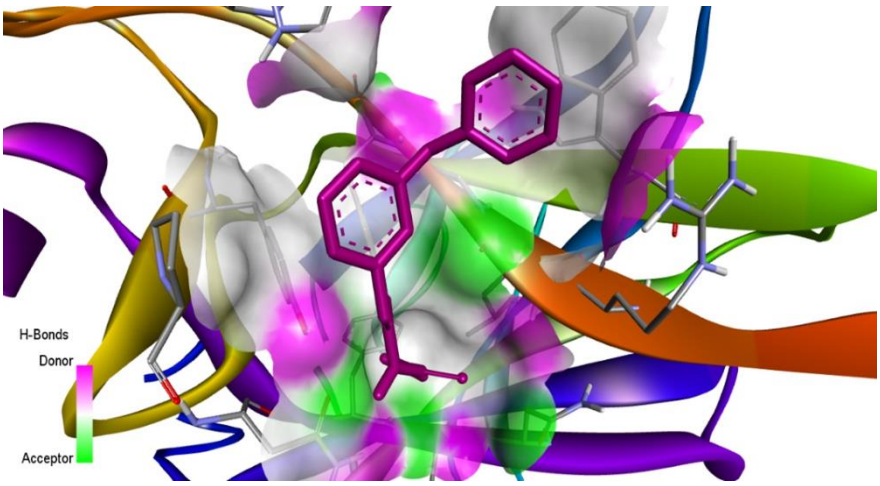

Figure 23. Hydrogen bond interaction plot showing interactions of Probe-L with 4L09 cancer mutant protein.

4. Conclusions

In summary, we have synthesized and characterized the simple fluorescent Probe (Probe -L). ^{1}H-NMR,^{13}C-NMR, and LC-MS data support the structure of Probe-L. Probe –L showed the turn-on fluorescent behavior with Pb^{2+} ions in acetonitrile solution. Probe –L also showed fluorescence enhancement upon binding with Pb^{2+}. The Probe-L was found to be an excellent fluorescent chemo sensor in the pH range of 5.0 to 13.0. Molecular docking investigations also reveal that the Probe-L interacts effectively with BSA and p53 cancer mutant protein with binding scores of -7.4 and -6.0 kcal/mol, respectively.

Funding

This research work received no external funding.

Acknowledgments

The author M Prema, is sincerely thankful to OBC cell, University of Mysore, for the award of fellowship and also to Institute of Excellence, Vijnana Bhavana, University of Mysore, Manasagangotri, Mysuru, for providing the spectral data.

Conflicts of Interest

The authors declare no conflict of interest.

References

1. Niu, X.; Zhong, Y.; Chen, R.; Wang, F.; Liu, Y.; Luo, D.; A “turn on” fluorescence sensor for Pb^{2+} detection based on graphene quantum dots and gold nanoparticles. *Sensors and actuators B: Chemical* **2018**, *255*, 1577-1581, http://dx.doi.org/10.1016/j.snb.2017.08.167.
2. Deng, Y.; Chen, Y. and Zhou, X. Simultaneous Sensitive Detection of Lead (II), Mercury (II) and Silver Ions Using a New Nucleic Acid-Based Fluorescence Sensor. *Acta Chim. Slov* **2018**, *65*, 271–277, https://doi.org/10.17344/acsi.2017.3620.
3. Kuang, H.; Xing, C.; Hao, C.; Liu, L.; Wang, L. and Xu, C. Rapid and Highly Sensitive Detection of Lead Ions in Drinking Water Based on a Strip Immunosensor. *Sensors* **2013**, *13*, 4214-4224, https://doi.org/10.3390/s130404214.
4. Gua, Y.; Huang Z.; Zhu, De-L.; Shun- yu, H.; Li, H. and Chang-Yu, H. Anthocyanin biosynthetic pathway switched by metalloregulator PbrR to enable a biosensor for the detection of lead toxicity. *Front. Microbiol* **2022**, *13*, 1-10, https://doi.org/10.3389/fmicb.2022.975421.

5. Liu, Y.; Yang, H.; Wan, R.; Khan, M.R.; Wang.; Busquets, R..; Deng, R.; He, Q. and Zhao, Z. Ratiometric G-Quadruplex Assay for Robust Lead Detection in Food Samples. *Biosensors* **2021**, *11*, 274, 1-14, https://doi.org/10.3390/bios11080271.
6. Brown, B.; Kishna, S.; Heck, D. E. and Kim, H. D. Early Detection of the low dose Lead exposure prevents mental disorders using non-invasive fluorescence and multi-omics. *GSC Advanced Research and Reviews* **2022**, *12*, 120-125, https://doi.org/10.30574/gscarr.2022.12.1.0183.
7. Cai, Y.; Ren, B.; Peng, B.; Zhang, C. and Wei, X. Highly Sensitive and Selective Fluorescence "Turn-On" Detection of Pb(II) Based on Fe_3O_4@Au–FITC Nanocomposite. *Molecules* **2021**, *26*, 3180, 1-10, https://doi.org/10.3390/molecules26113180.
8. Xu, L.; Su, X.; Zhang, Q.; Li, X.; Chen, C.; Zhang, X. Y. ELISA and Chemiluminescent Enzyme Immunoassay for Sensitive and Specific Determination of Lead(II) in Water, Food and Feed Samples. *foods* **2020**, *9*, 1-10. https://doi.org/10.3390/foods9030305.
9. Deibler, K.; Basu, P.; Continuing issues with lead: Recent Advances in Detection. *Eur J Inorg Chem*. **2013**, *7*, 1086-1096, https://doi.org/10.1002/ejic.201200997.
10. Chen, H.; Shao, S.; Yu, Y.; Huang, Y.; Zhu, X.; Zhang, S.; Fan, J.; Yin, H.Y.; Chi, B.; Wan, M.; Mao, C. A dual-responsive biosensor for blood lead detection. *Analytica Chimica Acta*, **2020**, *1093*, 131-141, https://doi.org/10.1016/j.aca.2019.09.062
11. Salih, F. E.; Ouarzane, A.; Rhazi, M. E. Electrochemical detection of lead(II) at bismuth/Poly(1,8-diaminonaphthalene) modified carbon paste electrode. *Arabian Journal of* Chemistry **2017**, *10*, 596-603, http://doi.org/10.1016/j.arabjc.2015.08.021.
12. Zheng, Y.; Li, Q.; Wang, C. and Su, M. Enhanced Turn-on Fluorescent Detection of Aqueous Lead ions with Size- Shrinkable Hydrogels. *ACS Omega* **2021**, *6*, 11897-11901, https://doi.org/10.1021/acsomega.1c00150.
13. Kanegae, A.; Takata, Y.; Takashima, I.; Uchinomiya, S.; Kawagoe, R.; Usui, K.; Yamashita, A.; Wongkongkatep, J.; Sugimoto, M. and Ojida, A. A multicolor and ratiometric fluorescent sensing platform for metal ions based on arene–metal-ion contact. *comms chem* **2021**, *4*, 1-7, https://doi.org/10.1038/s42004-021-00541-y.
14. Song, R.; Zhang, Q.; Chu, Z. L.; Dai, H.; Wu, W. Fluorescent cellulose nanocrystals for the detection of lead ions in complete aqueous solution. *Cellulose* **2019,** *26*, 9553–9565, https://link.springer.com/article/10.1007/s10570-019-02760-y.
15. Ali, M.H.; Ahmed, O. S.; Bassem, H.; Heakal.; Younis, A.; Wael, M. A. and Mohamed, F. M. Green Synthesis, Characterization, Antimicrobial and Anticancer Screening of New Metal Complexes Incorporating Schiff Base. *ACS Omega* **2022**, *7*, 32418-32431, https://doi.org/10.1021/acsomega.2c03911.
16. Hanan, B. H.; Abeer, A. S.; Magda, H. A.; Amal, S.B. Synthesis, Spectroscopic Characterization and Biological Studies of Mn(II), Cu(II), Ni(II),Co(II) and Zn(II) Complexes with New Schiff Base of 2-((Pyrazine-2-ylimino)methyl)phenol. *Appl.Sci.***2021**, *11*, 1-16, https://doi.org/10.3390/app11199067.
17. Saad, I. B.; Hannachi, N.; Roisnel, T. and Hlel, F. Optical, UV-vis spectroscopy studies, electrical and dielectric properties of transition metal-based of the novel organic-inorganic hybrid. *Journal of advanced dielectrics*, **2019**, *9*, 1-15, https://doi.org/10.1142/S2010135X19500401.
18. Wolfe, A.; Shimer, G. H.; Meehan, T. Polycyclic aromatic hydrocarbons physically intercalate into duplex regions of denaturated DNA. *Biochemistry* **1987,** *26*, 6392-6396, https://doi.org/10.1021/bi00394a013.
19. Behera, S.; Behura, R.; Mohanty, P.; Sahoo, M.; Subramanya, R. D.; Verma, A. K.; Jali, B. R. Study of Interaction Between Bovine Serum Albumin and Dolutegravir Intermediate: Fluorescence and Molecular Docking Analysis. *Biointerface Research in Applied Chemistry* **2021**,*11*, 13102-13110, https://doi.org/10.33263/BRIAC115.1310213110.
20. Ziya, A. A Turn-on Fluorescent Sensor For Cadmium Ion Detection In Aqueous Solutions. *JOTCSA* **2020**, *7*, 277-286, https://doi.org/10.18596/jotcsa.638912.
21. Sagirh, A.; Bozkurt, E. Rhodamine-Based Arylpropenone Azo Dyes as Dual Chemosensor for Cu^{2+}/ Fe^{3+} Detection. *Journal of Photochemistry and Photobology A:Chemistry* **2020**, *403*,112836, http://doi.org/10.1016/j.jphotochem.2020.112836.
22. Li, C. L.; Lu, P. H.; Lin, S. Y.; Wu, A. T. A turn –on fluorescent chemosensor for the recognition of Pb^{2+}. *Journal of Photochemistry and Photobiology A*: Chemistry **2019,** *385*, 112088, 1-6, https://doi.org/10.1016/j.jphotochem.2019.112088.
23. Gupta, V. K.; Singh, A. K.; Kumawat, L. K. Thiazole Schiff base turn-on fluorescent chemosensor for Al^{3+} ion. *Sensors and Actuators B* **2014**, 195, 98-108, http://dx.doi.org/10.1016/j.snb.2013.12.092.
24. Al-hazmi, H. A.; Ahsan, W.; Ibrahim, A. M. M.; Khubrani, R.A.Y.; Haddadi, Z.A.A.; Safhi, A.Y.F.; Shubayr, N.; Bratty, M. A.; Najmi, A. Investigation of bovine serum albumin aggregation upon exposure to silver(I) and copper(II) metal ions using Zetasizer. *Open Chemistry* **2021**, *19*, 987-997, https://doi.org/10.1515/chem-2021-0089.
25. Wani, T.A.; Al-Rabiah, H.; Bakheit, A. H.; Kalam, M.A. and Zergar, S. Study of binding interaction of rivaroxaban with bovine serum albumin using multi-spectroscopic and molecular docking approach. *Chemistry Central Journal* **2017**, *11*,134, 1-9, https://doi.org/10.1186/s13065-017-0366-1.

26. Abeydeera, N.; Perera, I. C. and Perera, T. Synthesis, Characterization and BSA –binding studies of Novel Sulfonated Zinc-Triazine Complexes. *Bioinorganic Chemistry and Applications* **2018**, *2018*, 1-7, https://doi.org/10.1155/2018/7563820.
27. Sukri, S. A. M.; Heng, L. Y.; Karim, N. H. Synthesis, Characterization and DNA-Binding Studies of Hydroxyl Functionalized Platinum(II)Salphen Complexes. *J Fluoresc* **2017**, *27*, 1009-1023, https://doi.org/10.1007/s10895-017-2035-0.
28. Demir, B. S.; Ince, S.; Yilmaz, M.K.; Sezan, A.; Derinoz, E.; Tok, T.; Saygideger, Y. DNA Binding and Anticancer Properties of New Pd(II)-Phosphorus Schiff Base Metal Complexes.*Pharmaceutics***2022**, *14*, 2409, https://doi.org/10.3390/pharmaceutics14112409.
29. Prakash, G.; Shiva Prasad, K.; Ibrahim, S.; Revanasiddappa, H. D. Novel Benzimidazole Derived Imine-Based Ligand and its Co(III), Ni(II),Cu(II) and Pt(II) Complexes: Chemical Synthesis, Structure, Antimicrobial, DNA Interaction Studies and Nuclease Activity. *Lett. Appl. NanoBioscience***2020**, *9*, 1655-1672, https://doi.org/10.33263/LIANBS94.16551672.
30. Baskaran, S.; Krishnan, M. M.; Arumugham, M. N.; Kumar, R. DFT Analysis and DNA binding, cleavage of copper(II)complexes. *Journal of Molecular Liquids* **2016**, *221*,1045-1053, https://doi.org/10.1016/j.molliq.2016.06.055.
31. Prashanth, M. K.; Madaiah, M.; Revanasiddappa, H. D. and Amruthesh, K. N. Synthesis, Characterization and BSA Binding Studies of Some New Benzamides Related to Schiff Base. *Hindawi Publishing Corporation* **2013**, *2013*,1-12, http://dx.doi.org/10.1155/2013/791591.
32. Bermanm, H. M.; Westbrook, J.; Feng, Z.; Gilliland, G.; Bhat, T. N.; Weissing, H.; Shindyalov, I. N. and Bourne, P. E. The protein data bank. *Nucleic Acid Research* **2000**, *28*, 235-242, https://doi.org/10.1093/nar/28.1.235.
33. Theerawatanasirikul, S.; Semkum, P.; Lueangaramkul, V.; Chankeeree, P.; Thangthamniyom, N. and Kcharoenusk, P.L. Non- Nucleoside Inhibitors Decrease Virus Replication by Blocking the Viral $3D^{pol}$. *Viruses* **2023**, *15*, 124, http://doi.org/10.3390/v15010124.
34. BIOVIA, Dassault Systemes, *BIOVIA Discovery Studio Visualizer*, v21, San Diego: Dassault systemes, **2021**, https://www.3ds.com/products-services/biovia/products/molecular-modeling-simulation/biovia-discovery-studio/.
35. The PyMOL Molecular Graphics System, Version 2.5.2 Schrodinder, LLC, https://pymol.org/2/.
36. Dewangan, D.; Vaishnav, Y.; Mishra, A.; Jha,A.K.; Verma,S. ; Badwaik, H. Synthesis, molecular docking and biological evaluation of Schiff base hybrids of 1,2,4-triazole-pyridine as dihydrofolate reductase inhibitors. *Current research in pharmacology and drug discovery* **2021**, *2*, 1-7, https://doi.org/10.1016/j.crphar.2021.100024.
37. Soliman, E.; Ibrahim, M.M.; Khously, M.E.; Mehaseeb, I, E.; Ramdan, A. E. M.; Mahfouz, M. E.; Shaban, S.Y.; Eldik, R.V. BSA Interaction, Molecular Docking and Antibacterial Activity of Zinc(II) Compolexes Containing the Sterically Demanding Biomimetic N_3S_2 Ligand: The Effect of Structure Flexibility. *Molecules* **2022**, *27*, 3543, https://doi.org/10.3390/molecules27113543.

Supplementary materials

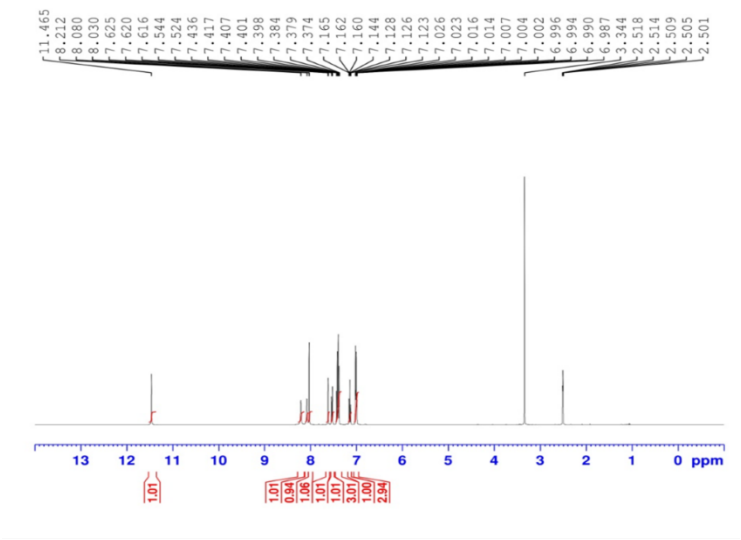

Figure S1.[1]H NMR spectrum of Probe-L

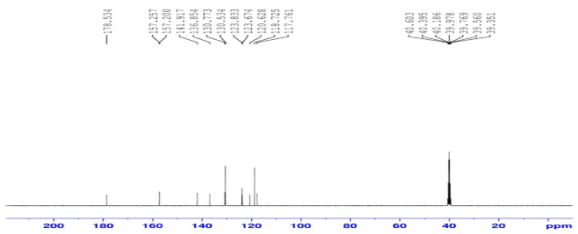

Figure S2. [13]C NMR spectrum of Probe-L

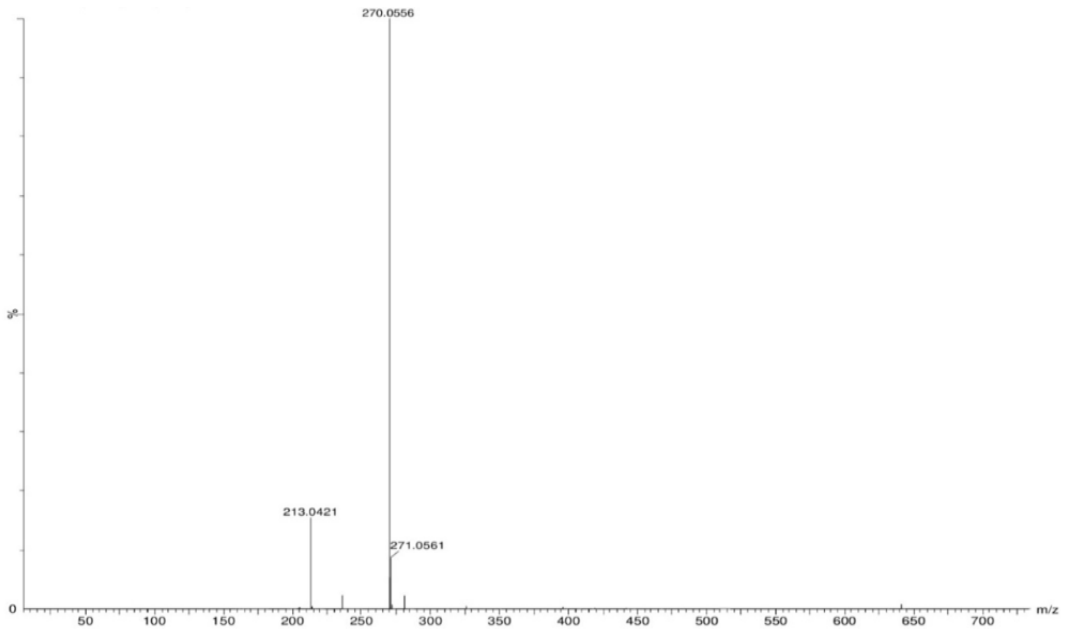

Figure S3. Mass spectrum of Probe-L

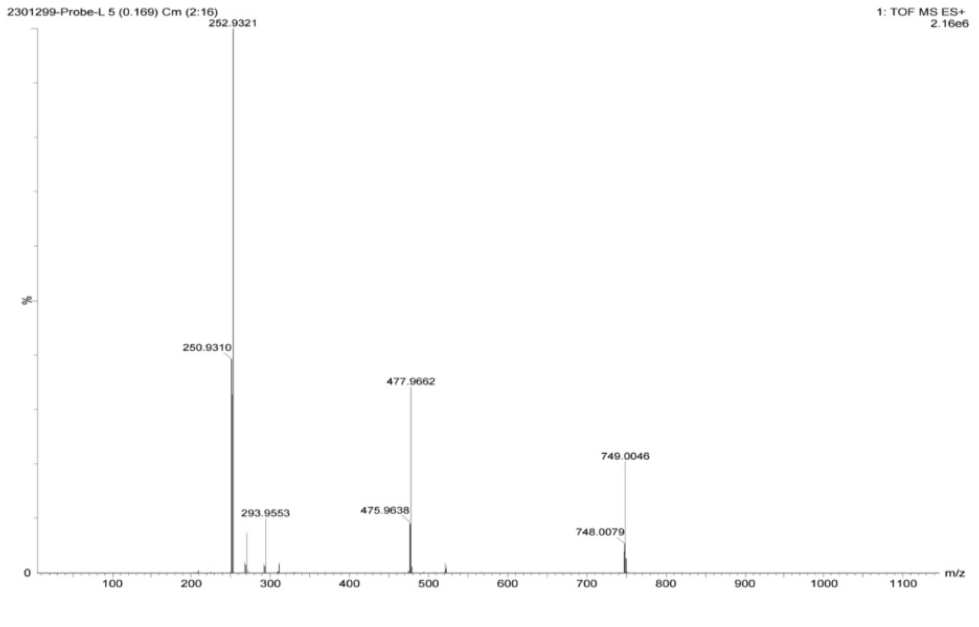

Figure S4. Mass spectrum of Pb^{2+} complex

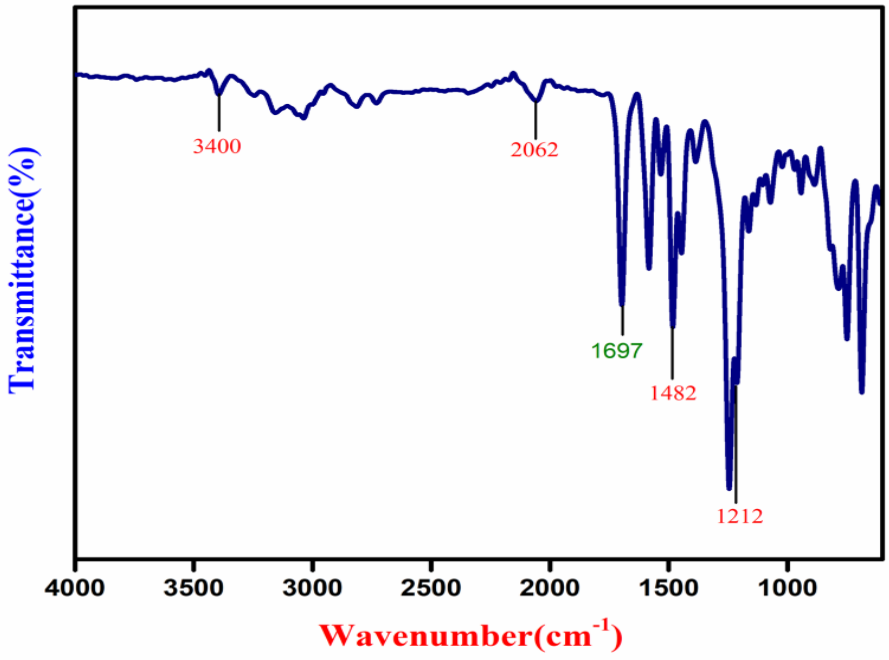

Figure S5. FT-IR spectra of Probe-L

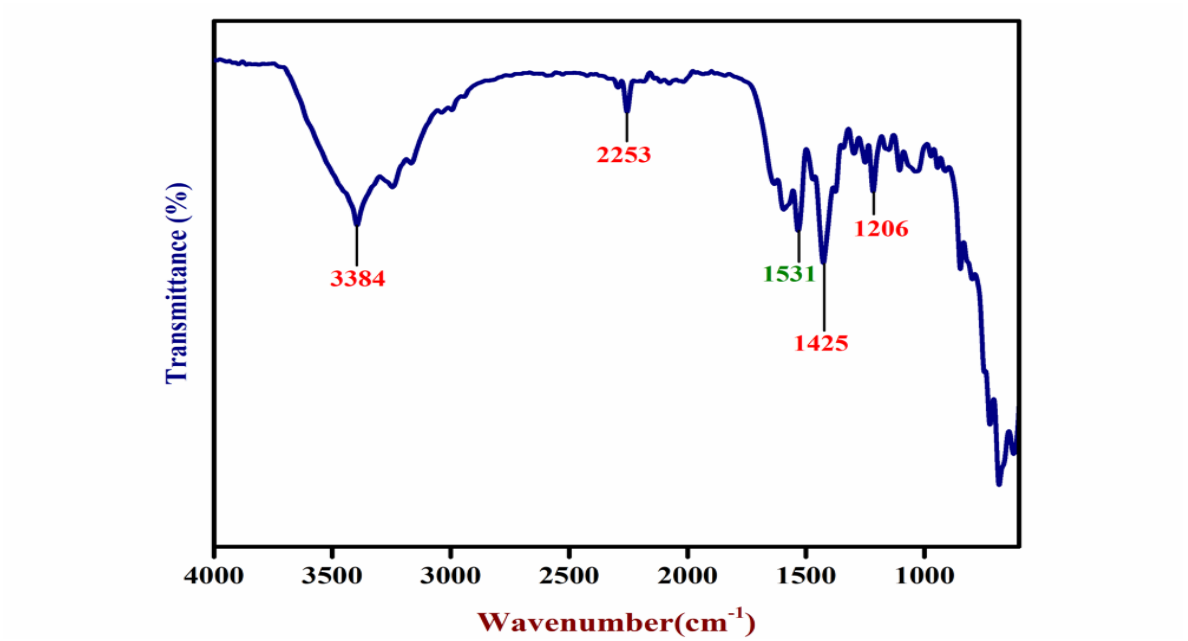

Figure S6. FT-IR spectra of Pb^{2+} complex.